Solution-Phase Synthesis and Electrochemical Hydrogen Storage of Ultra-Long Single-Crystal Selenium Submicrotubes

Bin Zhang, Wei Dai, Xingchen Ye, Weiyi Hou, and Yi Xie*

Department of Nanomaterials and Nanochemistry, Hefei National Laboratory for Physical Sciences at Microscale, University of Science and Technology of China, Hefei 230026, P. R. China

Received: July 29, 2005; In Final Form: October 15, 2005

Ultra-long single-crystalline trigonal selenium submicrotubes were synthesized using a facile one-step solution-phase approach with the assistance of nonionic surfactant Polyoxyethylene(20)sorbitan monolaurate (Tween-20), which turned out to be significant for the formation of ultra-long Se submicrotubes. XRD, Raman, SEM, and TEM were adopted to characterize the morphology, structure and phase composition of the as-prepared Se products. It was found that the length of the obtained Se submicrotubes was over 100 μm. By variation of the experimental parameters, the t-Se spheres, nanowires, and broken microtubes can be prepared. The possible growth mechanism of the ultra-long selenium submicrotubes was explained. In addition, we have also demonstrated that the synthesized ultra-long t-Se submicrotubes using the Tween-20-assisted approach can electrochemically charge and discharge with the high capacity of 265 mAh/g (corresponding to 0.97 wt % hydrogen in SWNTs) under normal atmosphere at room temperature. Cyclic voltammetry was adopted to investigate the adsorption−oxidation behavior of ultra-long selenium submicrotubes. It was observed that the morphology of the synthesized selenium products had a remarkable influence on their capacity of electrochemical hydrogen storage. These differences in hydrogen storage capacity are likely due to the size and density of tubes as well as the microcosmic morphology of different Se samples. The as-obtained ultra-long Se submicrotubes are expected to find wide applications in hydrogen storage, high-energy batteries, and optoelectronic, biologic, and catalytic fields as well as in the studies of structure−property relationships. This simple Tween-assisted approach might be extended to the preparations of one-dimensional nanostructures of tellurium and other anisotropic materials.

Introduction

During the past few decades, much attention has been focused on one-dimensional (1D) nanostructures, such as nanowires, nanorods, nanobelts, and nanotubes, owing to their fundamental significance in investigating the dependence of various physical properties on dimensionality and size reduction, as well as their potential applications in many fields.[1−3] Since the discovery of carbon nanotubes in 1991,[4] intense interest has been initiated to design novel methods to synthesize inorganic tubes. However, most investigations have been concentrated on the compounds with layered or quasi-layered structure.[5−7] Emphatically, there are few reports on the synthesis of single-crystalline semiconductor tubular materials. For the preparation of nanotubes/submicrotubes with nonlayered structures, template-assisted route is still considered as a potential and effective method.[8,9]

Among various semiconductor materials, trigonal selenium (t-Se) is well-known as a valuable material with good photoelectric, catalytic, semiconducting properties, and attractive commercial use in photocopiers, rectifiers and xerography. Moreover, trigonal selenium attracts wide research interest because the extended spherical chains of Se atoms in the trigonal phase can be a natural template to guide the growth preferentially along the *c*-axis.[10,11] Consequently, it is logical to expect that the novel t-Se structure may be important both in theoretical studies and in technological applications, especially in constructing the semiconductor-based devices. At present, a wealth of intriguing 1D Se materials have been synthesized.[12−24] Trigonal selenium nanorods of high purity have been fabricated using laser ablation of selenium powders[12] as well as the reduction of selenious acid under ultrasonic irradiation.[13] The t-selenium nanowires are also created by sonochemical approach[14] and the solution-mediated transformation from Se powders or semiconductor nanoparticles.[15] CVD was utilized to prepare hexagonal selenium nanowires with the assistance of silicon as the catalyst.[16] Interestingly, Xie et al. found that selenium microballs with monoclinic structure could form t-Se nanorods in ethanol solutions.[17] In a recent report, we also fabricated t-Se nanoribbons and nanowires network using the CVD method.[18] Emphatically, Xia's group took advantage of t-Se nanowires as the templates to successfully prepare CdSe and Pt nanotubes,[19−20] and this thought-provoking work may offer an important method to synthesize other materials with hollow structure and will broaden the application of Se materials. Recently, much attention has been devoted to the synthesis of tubular selenium.[21−24] In our group, Se microtubes with ca. 1−1.5 mm in length, 15 μm in diameter, and 5 μm in thickness were fabricated by dissolving Se powders in different organic solvents at mild temperatures.[21] Se nanotubes of good quality were also prepared by reducing the as-prepared precursor of Na_2SeSO_3 in the micelles of $C_{12}E_{23}$ under acidic condition, assisted by additional ultrasonic bath.[22] Selenium salts are used as Se source to fabricate the irregular or broken tubular structure.[23] In a very recent report, Se tubes are also synthesized via a three-step method.[24] However, to the best of our

* To whom correspondence should be addressed. Telephone and Fax: 86-551-3603987. E-mail: yxie@ustc.edu.cn.

10.1021/jp054214k CCC: $30.25
Published on Web 11/12/2005

knowledge, there have been few reports on the regular single-crystalline selenium submicrotubes, especially these whose diameter is longer than 10 μm, through simple one-step synthesis route.

As for various materials, one of the challenging and intriguing problems is to find/study their potential properties and thus to achieve materials' applications in life-relating fields. Energy crisis are considered to be one of the most troublesome embarrassments in current world. Hydrogen-based energy is well-known as an effective alternative for the fossil-fuel-dominated energy, but the crux is how to synthesize materials with high hydrogen uptake.[25] Electrochemical storage of hydrogen is found to be a good method because of the relative low temperature and high stability. It has been observed that layered-like materials[26−30] (eg. CNT, BN nanotubes, MoS_2 nanotubes, TiS_2 nanotubes) have attracting hydrogen storage capacity. However, the electrochemical hydrogen storage investigations of materials with chainlike or quasi-layered structure are still vacant. As mentioned above, selenium atoms in infinite spiral chains parallel to the *c*-axis in the trigonal phase are bound with covalent bonds, whereas the chains are packed into a hexagonal lattice through van der Waals' interactions.[18] We preliminarily assume that the interstitial sites among Se chains and the pores of Se submicrotubes may potentially store hydrogen, which function similar to those of layered nanotubes. Therefore, the electrochemical hydrogen storage behavior of ultra-long Se submicrotubes deserves our special research efforts.

Herein, we report for the first time a facile one-step hydrothermal method for the fabrication of ultra-long single-crystalline Se submicrotubes using SeO_2 as the selenium source with the assistance of nonionic surfactant Polyoxyethylene(20) sorbitan monolaurate (Tween-20). It is observed that the length of the as-prepared submicrotubes is over 100 μm. The possible formation mechanism of t-Se submicrotubes is presented. This novel soft template route can be potentially extended to fabricate submicrotubes of Te and other anisotropic materials. Other similar nonionic surfactants (eg. Span-20, Span-40, Span-60, Span-85, and other Tween series) are expected to serve as the soft templates to synthesize Se tubes in our approach, and the size and diameter of Se tubes may be modulated by varying the surfactants and their molar ratio to selenium. In addition, we have demonstrated that the ultra-long selenium submicrotubes can electrochemically charge and discharge with the high capacity of 265 mAh/g (amounts to 0.97 wt % hydrogen in SWNTs[26−30]) at room temperature. The electrochemical discharge capacities of Se nanomaterials with different morphologies were also investigated. It is found that the discharge capacity is sensitive to the morphologies and the diameters of Se tubular materials. Furthermore, the preparation and electrochemical studies of Se nanomaterials will offer great opportunities to explore the dependence of novel properties of material on its morphology and is essential to manufacturing potential optoelectronic devices. The obtained ultra-long selenium submicrotubes are expected to find wide applications in hydrogen storage, high-energy batteries, and catalytic fields.

Experimental Section

Chemicals. All the chemicals were of analytical grade and were used as received. Aqueous solutions were prepared using distilled water.

Preparation of Ultra-Long Se Submicrotubes. In a typical procedure, 0.4 g of SeO_2 and 1 mL of Tween-20 were first added to 20 mL of distilled water, and the mixture was dispersed to form a homogeneous solution under constant strong stir. Then 0.5 mL of hydrazine hydrate ($N_2H_4 \cdot H_2O$, 85%) was slowly dropped into the above solution at room temperature, and the solution became brick red quickly, indicating the formation of amorphous selenium (a-Se) spherical particles.[10−11] After reacting for 15 min while giving out the gas (N_2) yielded in the evolution, the resulting solution was transferred into a 50 mL Teflon-lined autoclave. The autoclave was sealed, maintained at 120 °C for 24 h, and cooled to room-temperature naturally. The black precipitate was collected and washed for three times with absolute ethanol and distilled water, respectively. Then the sample was dried in a vacuum at 50 °C for 6 h.

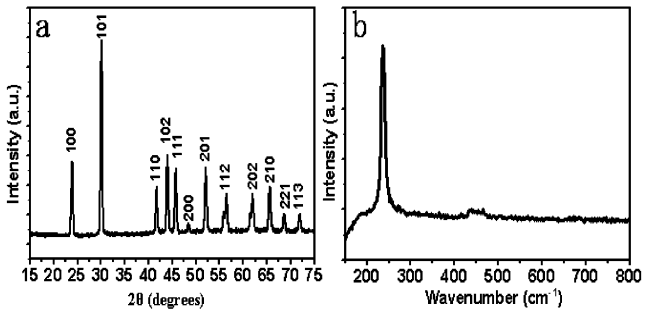

Figure 1. (a) XRD pattern of the as-prepared Se submicrotubes. All the diffraction peaks can be indexed according to trigonal Se, indicating the high crystallinity and the preferential growth along [001] direction. (b) Raman scattering spectrum of the selenium submicrotubes. The resonance peak at 236.3 cm^{-1} is a characteristic stretching mode of t-Se, revealing the nature of trigonal phase of the obtained Se submicrotubes.

Characterization with SEM, XRD, Raman, and TEM. The X-ray diffraction patterns (XRD) of the products were recorded with a Rigaku Dmax diffraction system using a Cu Kα source ($\lambda = 0.154178$ nm). The scanning electron microscopy (FESEM) images were taken with a JEOL-JSM-6700F field emitting scanning electron microscope (FE-SEM, 15 kV). Transmission electron microscopy (TEM) images and electron diffraction pattern were obtained with Hitachi 800 system at 200 kV. The specimens of TEM measurements were prepared via spreading a droplet of ethanol suspension onto a copper grid, coated with a thin layer of amorphous carbon film, and allowed to dry in air.

Electrochemical Measurements. The electrochemical measurements were carried out following the method reported in ref 26 with slight modifications. Briefly, the electrode was fabricated by directly pressing the prepared selenium samples on a sheet of nickel foam at 50 MPa. All the experiments were performed in a three-electrode cell in 5 M KOH at 25 °C under ambient pressure. The Se submicrotubes products were used as the working electrode, $Ni(OH)_2$/NiOOH was used as the counter electrode, and Hg/HgO was used as the reference electrode. The obtained Se submicrotubes electrode was charged for 3 h at a constant current density after a 2 s rest. The charging and discharging current density was controlled at 50 mA/g except for especial illumination. All the electrochemical hydrogen storage experiments were carried out using the Land battery system (CT2001A). The cyclic voltammetric (CV) measurements were carried out by an electrochemical workstation (CHI 660).

Results and Discussion

The crystal structure and phase composition of Se products were first characterized using X-ray powder diffraction (XRD). Figure 1a displays a representative XRD pattern of the as-

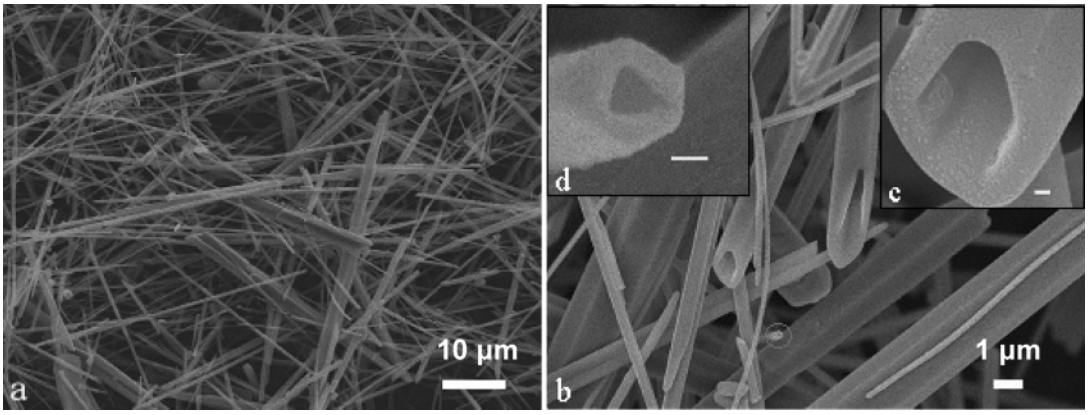

Figure 2. Typical FESEM images of the obtained t-Se submicrotubes. (a) at a low magnification, indicating that the ultra-long t-Se submicrotubes can be fabricated on a large scale. (b) at a high magnification, revealing the tubular shape of the Se samples. (c, d) at a higher magnification, further confirming the tubular morphology. Scale bars (c, d): 100 nm.

prepared Se samples, suggesting their high crystallinity. All the diffraction peaks can be readily indexed to the triagonal phase of selenium (JCPDS 06-362). The abnormal intensity of (100) peaks clearly indicates that these t-Se products had predominately developed along the unique [001] direction, which is parallel to the helical chains of Se atoms or the *c* axis.

Raman spectroscopy has been proven to be a powerful tool to analyze the phase of Se materials due to their characteristic signals in the spectrum.[31] Typically, the resonance peak of t-Se is located at ~235 cm^{-1} whereas those of amorphous selenium and monoclinic selenium are centered at ca. 250 and ca. 260 cm^{-1}, respectively.[31] As shown in Figure 1b, only one peak at 236 cm^{-1} was observed in the frequency region between 200 and 300 cm^{-1}, which was assigned to the characteristic mode of t-Se. This testifies that the as-prepared Se products have a high crystal quality, as revealed in the XRD data.

The morphology of the obtained Se products was characterized using field emission scanning electron microscopy (FESEM) and the typical FESEM images are displayed in Figure 2. From the low magnification FESEM image (Figure 2a), the as-prepared Se submicrotubes are relatively uniform and can be fabricated on a large scale by this simple Tween-20-assisted solution approach. This higher-magnification FESEM image in Figure 2b clearly manifests the product's tubular structure. Figure 2c shows that the wall thickness of the bigger Se tubes is about 120 nm, whereas the wall thickness of small *t*-Se nanotube is ca. 40 nm (Figure 2d). Also from Figure 2, it can be seen that the lengths of Se tubes are over 100 μm, implying that ultra-long selenium submicrotubes have been successfully synthesized on a large scale by our presented method.

The morphology and structure of the t-Se submicrotubes products are further detected by transmission electron microscopy (TEM) and selected area electron diffraction (SAED). Figure 3a displays the typical TEM image of the obtained selenium product, revealing that the obtained sample has a tubular morphology with a uniform thickness of ca. 120 nm, in good agreement with the FESEM image in Figure 2. Figure 3b shows the associated SAED pattern of the Se submicrotubes, recorded with the incident electron beam perpendicular to the wide surface of the submicrotube. The index of the spots in the SAED pattern indicates that the submicrotubes is a single crystal and predominantly grows along the [001] direction (*c*-axis), consistent with previous observations on Se 1D nanomaterials.[10−20] Through extensive investigations on individual submicrotubes from selenium products with SAED, we found that this orientation was maintained in all of the products. Figure 3c also gives the TEM image of the t-Se submicrotube with

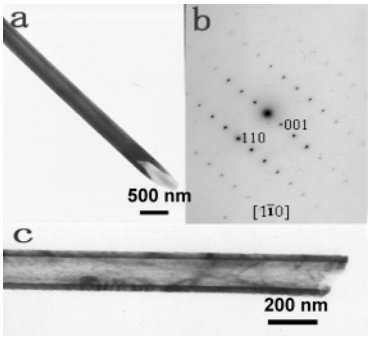

Figure 3. (a, b) Representative TEM image of one t-Se submicrotube and the associated SAED pattern, showing that the thickness of tube wall is ca. 120 nm. The [1$\bar{1}$0] zone axis of the trigonal selenium submicrotube was identified, indicating the preferential growth along [001] direction. (c) Typical TEM image of one small t-Se submicrotube, showing that the thickness of tube is about 40 nm.

relatively small diameter, suggesting that its wall thickness is uniform and lower (ca. 40 nm) than that of big submicrotubes. The SAED measurements also indicate that the small selenium submicrotubes preferentially developed along the [001] direction. The SEM, XRD, TEM, and Raman spectroscopic results demonstrate that t-Se submicrotubes with high crystallinity and purity can be successfully synthesized by using the Tween-assisted hydrothermal method.

To ascertain the effect of the nonionic surfactant on the morphology, a series of parallel experiments were performed. In the absence of Tween-20, while other conditions remains unchanged, it was found that Se submicrotubes cannot be obtained, and the as-prepared products are selenium spheres (Figure 4a), suggesting that tween-20 is necessary for the formation of t-Se tubes. When the volume of Tween-20 was increased to 2 mL, the obtained samples are broken Se microtubes with ca. 5−10 μm in diameter, 20−80 μm in length (Figure 4b). Compared with the ultra-long Se submicrotubes, the diameter of the broken selenium microtubes become bigger while their length being shorter. We founded that the appropriate amount of Tween-20 for the synthesis of tubular selenium structure is 1.5−3 mL. When the hydrothermal temperature was controlled at 90 °C, selenium nanowires were obtained and a small quantity of cross-like junctions could also be observed in the final wire-like products, as shown in Figure 4c, indicating that the reaction temperature is a critical factor for the formation of Se submicrotubes.

Although the exact mechanism for the surfactant-modulated formation of ultra-long t-selenium submicrotubes is still under

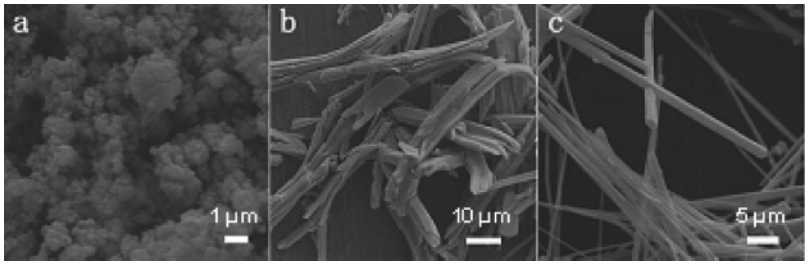

Figure 4. FESEM images of the obtained samples in different conditions: (a) t-Se spheres prepared from 0.4 g of SeO_2, 0 mL of Tween-20, and 20 mL of H_2O for 24 h at 120 °C under hydrothermal condition; (b) broken t-Se microtubes synthesized from 0.4 g of SeO_2, 2 mL of Tween-20 and 20 mL of H_2O for 24 at 120 °C under hydrothermal condition; (c) t-Se nanowires produced 0.4 g of SeO_2, 2 mL of Tween-20 and 20 mL of H_2O for 24 h at 90 °C under hydrothermal condition. In Figure 4c, a small quantity of cross-like junctions can be observed.

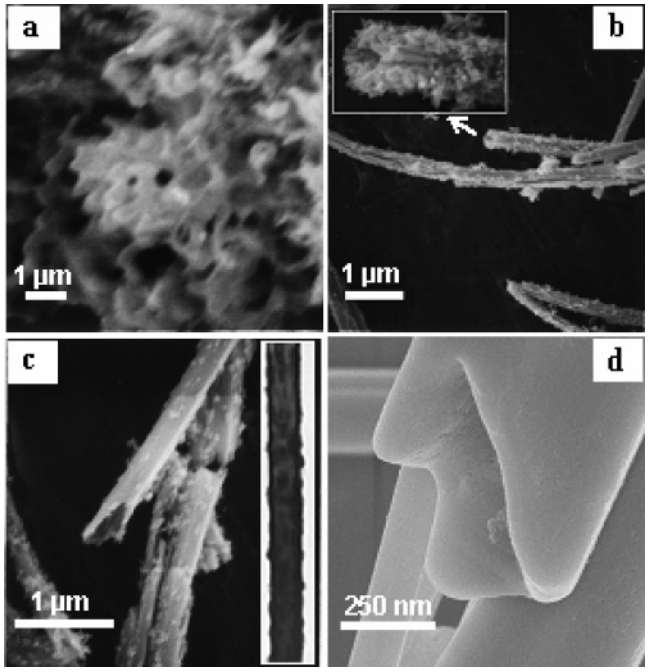

Figure 5. SEM image of the as-prepared Se samples collected at different hydrothermal time: (a) 0 h, collected quickly after hydrazine hydrate was added to the reaction mixture; (b) 0.5 h, the inset is a higher magnification of SEM, reflecting the particles composition of selenium tube; (c) 2 h, the right inset showing TEM image of one tube; (d) 24 h.

investigation, the directing role of Tween-20 is undoubtedly significant. In the absence of Tween-20, the synthesized products were not the selenium tubular structure, but the spherelike Se particles, as seen in Figure 4a. To understand the growth mechanism of ultra-long Se submicrotubes, four samples at different reaction stages were collected. Figure 5a shows the SEM image of the Se samples collected quickly after 0.5 mL of hydrazine hydrate ($N_2H_4 \cdot H_2O$) was added to the mixture of SeO_2, Tween-20 and H_2O. As demonstrated in Figure 5a, the products mainly consisted of spherical nanoparticles and series-sphere-joined aggregates. Further Raman spectroscopic analysis (not shown here) shows that the intermediates are composed of the coexistence of t-Se and a-Se phase, suggesting that SeO_2 was rapidly reduced to the coexistence of Se spheres and quasi-1D nanomaterials by N_2H_4 in the presence of Tween-20. Similar results of the coexistence of two kinds of Se phases have been reported by Xia et al. in preparing Se nanowires on the basis of TEM observations.[10] Owing to the very unstable properties of amorphous selenium spheres under current approach, it is difficult to obtain the pure spherical Se particles, but it is reasonable to think that the SeO_2 is first reduced to form amorphorous selenium particles (a-Se) and then these Se spheres partly dissolved and transformed into the series-sphere-joined aggregates because of the Se anisotropic nature. When the hydrothermal reaction was processed for 0.5 h, the as-prepared products are Se submicrotubes with rough outer surface, as displayed in Figure 5b. A higher SEM image clearly manifests that many particles and spheres-linked aggregates coexist in the outer surface of Se tubes along a certain direction (the inset in Figure 5b). With the reaction time increased to 2 h, the tubular morphology of the Se submicrotubes becomes obvious (Figure 5c), and their crystallinity also becomes better. However, there are still a few particles at the outer wall of selenium submicrotubes, which are further confirmed by the TEM image inserted in Figure 5c. In the following process, the crystallinity of Se tube is increased with the prolonged reaction time. When the hydrothermal reaction continues for 24 h, the outer surface of Se submicrotubes is quite smooth (learned from the SEM image in Figure 5d), indicating the high crystallinity. XRD and SAED measurements show that the ultra-long selenium has a preferential growth along the [001] direction. We believe that Tween-20 micelles play a very important role in the formation of Se submicrotubes. It was thought that a-Se spheres were first formed on the outer shell of Tween-20 micelles because of the good solubility for a-Se[22] as a result of much water entrapped by the poly(oxyethylene) chains of Tween-20. In the following process, the neighboring a-Se spheres at the outer shell of Tween-20-based micelles quickly dissolved and recrystallized along the [001] direction due to the inherently anisotropic structure of t-Se,[10−20] and then formed the tubular structure. Under the hydrothermal condition, the dissolved a-Se particles were diffused to the surface of Se submicrotubes, as revealed in Figure 5c, and provided the Se source for the durative growth to the ultra-long selenium submicrotubes. When the hydrothermal reaction continued, the selenium particles dissolved in the micelles were completely consumed and thus the crystallinity of Se submicrotubes became better. As for the formation of broken Se tubes and Se nanowires under other conditions, it was believed that the relative ratio of Tween-20 to the dissolved a-Se particles and the interstitial sites among the neighboring Tween micelles were mainly responsible for the difference in the as-prepared products' morphologies, similar to Qi's discussion.[22] It should be pointed out that the explanation for the growth process of ultra-long submicrotubes is rough, and more systematic work needs to be done to get a better knowledge on the formation mechanism, which is now underway in our group.

It was found that the ultra-long selenium submicrotubes had the function of electrochemical hydrogen storage. Figure 6 shows the charge−discharge voltage changes of ultra-long t-Se submicrotubes as a function of capacity at a constant current density at room temperature. In the charge curve of ultra-long t-Se submicrotubes (Figure 6a), one weak and perceptible

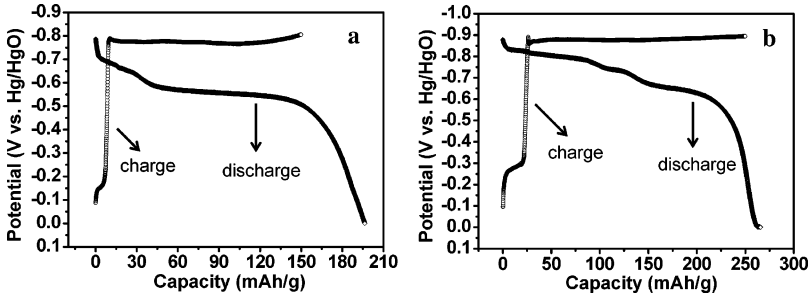

Figure 6. Charge-discharge curves of the ultra-long t-Se submicrotubes at a given constant current density: (a) 80 mA/g; (b) 50 mA/g.

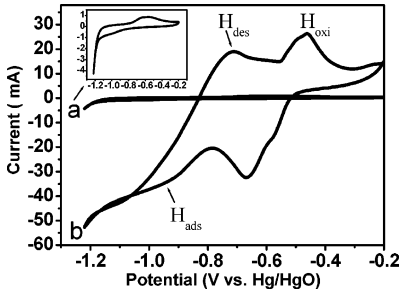

Figure 7. Cyclic voltammograms of the different electrodes in 5 M KOH at a sweep rate of 50 mV/s: (a) porous nickel; (b) ultra-long t-Se submicrotubes supported on the porous nickel substrate.

voltage plateau is seen at ca. 2 mAh/g. With the increase of the electrochemical capacity, the potential decreased quickly, but remain unchanged when the charge capacity reaches 14 mAh/g. One new obvious plateau of potential is observed between 14 and 150 mAh/g. This indicates that two different hydrogen adsorption sites[25] exist in the synthesized ultra-long selenium submicrotubes, in other words, there are two different electrochemical steps in the charging process. It is assumed that the H was first adsorbed into the pores/inner walls of selenium submicrotubes and then diffused into the interstitial sites among the Se chains, which is similar to the hydrogen storage mechanism of single-walled carbon nanotubes proposed on the basis of the density-functional calculation.[32] This two plateaus phenomenon become more obvious (Figure 6b) when the charge current density was decreased from 80 to 50 mA/g, suggesting that the charge current density has an important effect on the charge behaviors of Se submicrotubes, which may be related to the electrochemical diffusion and adsorption kinetics. As shown in Figure 6a, the plateau of the discharging potential is observed at ca. −0.58 V and the discharging capacity of 200 mAh/g can be obtained, which amounts to a hydrogen storage capacity of 0.74 wt % in SWNTs.[26−30] When the constant current density becomes 50 mA/g, the discharge voltage plateau is not distinct and the discharge capacity was increased to 265 mAh/g (corresponds to 0.97 wt % hydrogen in SWNTs, Figure 6b), revealing that the capacity of electrochemical hydrogen storage of the ultra-long Se tubes is sensitive to the charge−discharge current density. The value of discharging capacity is higher than those of MoS_2 and BN nanotubes.[27,28] The high capacity was considered to be pertinent to the enhanced electrocatalytic activity of the highly porous of selenium tubular structure and the weak van der Waals' interactions among infinite spiral chains. This indicates that ultra-long t-Se submicrotubes can be potentially applied as the material of electrochemical hydrogen storage.

Cyclic voltammograms (CVs) were also performed to further investigate the electrochemical hydrogen adsorption−desorption behaviors of porous Ni and ultra-long selenium submicrotubes supported on the porous nickel substrate. In the CV of the porous nickel electrode (the inset in Figure 7a), one broad oxidation peak of hydrogen is observed at ca. −0.55 V vs Hg/HgO, and one desorption peak of hydrogen can be found around −0.92 V, which are typical CV behaviors of nickel. When the working electrode was replaced by the ultra-long t-Se submicrotubes supported on the porous nickel substrate, the anodic oxidation peak of hydrogen appears at about −0.47 V (Figure 7b). As shown in Figure 7b, the hydrogen desorption peak can also be observed prior to hydrogen oxidation peak, indicating the possible existence of the strong chemisorption of hydrogen, similar to the observations and discussion on CVs of BN nanotubes.[28] In the following cathodic process, one adsorption peak of hydrogen appears at about −0.94 V (close to the values of the BN and MoS_2 nanotubes[27,28]). Interestingly, one new current peak (not observed in the previous CV investigations[25−28] of CNT, MoS_2 and BN nanotubes) can be clearly seen at ca. −0.67 V, which is probably attributed to the weak adsorption of hydrogen on the Se tubes or the reduction peaks of hydrogen. As for the charge−discharge mechanism of selenium submicrotubes, a simple scheme on the adsorption and release of hydrogen was tentatively displayed as shown in Scheme 1.

To study the morphology effect of t-Se on the capacity of electrochemically hydrogen storage, the charge−discharge curves of the synthesized broken selenium microtubes and spherelike Se particles as a function of capacity at a constant current density of 50 mA/g under normal atmosphere were

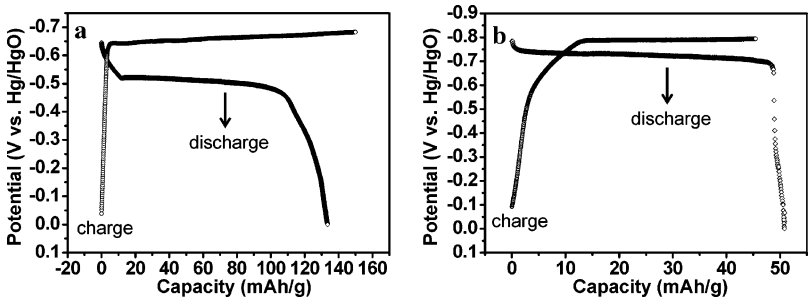

Figure 8. Charge-discharge curves of the broken Se microtubes (a, SEM image shown in Figure 4b) and spherelike Se particles (b, SEM image displayed in Figure 4a) at a given constant current density of 50 mA/g.

SCHEME 1. Electrochemical Hydrogen Storage of Ultra-Long t-Se Submicrotubes

$$Se + H_2O + x\ e^- \underset{\text{discharge}}{\overset{\text{charge}}{\rightleftharpoons}} (Se + H_{ad}) + x\ OH^-$$

measured and are shown in Figure 8. For the broken selenium microtubes samples, the value of the discharge capacity is 132 mAh/g, whereas the discharge capacity of spherelike Se particles is only 52 mAh/g. This manifests that the morphologies have exerted a noticeable influence on the electrochemical hydrogen storage ability of Se samples and also indicates that the tubular structure of selenium products is a crucial factor for the high hydrogen storage ability of Se tubes. Different from the ultra-long Se submicrotubes, only one voltage plateau in the charge curves was seen in broken selenium microtubes and Se particles. We believe that the tubular structure and the tube's diameter of selenium samples mainly contribute to the differences in the charging process. For the broken Se microtubes, the H atom may rapidly diffuse to the inter walls in a very short time owing to the microscale diameter of tube. It is well-known that the electrochemical capacity is a direct proportion function of the charging time. Therefore, the charging capacity in the process of hydrogen adsorbed into the pores/inter walls of selenium microtubes is rather small, and thus the corresponding potential plateau is invisible in the charging curve. As for the spherelike Se particles, there is only a diffusion process between layers of selenium chains (weak van der Waals' interactions) because of the absence of pores or tubes.

Conclusions

We have demonstrated a simple and practical solution-phase route to trigonal phase ultra-long selenium submicrotubes with the assistance of Tween-20. The SEM observations show that the final products were the t-Se tubular structure with a length of over 100 μm. The high crystallinity and purity of the ultra-long selenium submicrotubes were confirmed by XRD, Raman and TEM studies. It was found that the prepared selenium submicrotubes had a preferential growth along the [001] direction. By changing the experimental parameters, broken Se microtubes, Se nanowires, and spherelike particles were successfully synthesized. Interestingly, we also found that the ultra-long t-Se submicrotubes could store hydrogen in an electrochemical process. A high electrochemical discharge capacity of 265 mAh/g (amounts to 0.97 wt % hydrogen in SWNTs) was obtained at room temperature in the ultra-long Se submicrotubes electrode. For the ultra-long selenium submicrotubes, the phenomenon of two charging plateaus was seen. We deem that there are two steps in the process of hydrogen storage: the H was first adsorbed into the pores/inner-walls of selenium submicrotubes and then diffused into the interstitial sites among the Se chains. It has been demonstrated that the morphology of the synthesized Se products had a remarkable influence on the ability of electrochemical hydrogen storage. These differences in hydrogen storage capacity are likely due to the diameter and length of tubes as well as the microcosmic morphology of different selenium samples. The as-obtained ultra-long Se submicrotubes are expected to find wide applications in hydrogen storage, high-energy batteries, and optoelectronic, biologic, and catalytic fields as well as in the studies of structure−property relationships. In addition, ultra-long selenium submicrotubes might be used as the templates to produce other ultra-long one-dimensional functional nanomaterials. Importantly, by the same solution-phase approach, other similar nonionic surfactants (eg. Span-20, Span-40, Span-60, Span-85, and other Tween series) might potentially serve as the soft templates to synthesize submicrotubes/nanotubes of Se and other anisotropic materials with high electrochemical hydrogen storage capacity.

Acknowledgment. This work was financially supported by the National Natural Science Foundation of China. The authors acknowledge kind help from Mr. Linfeng Fei at USTC with TEM measurements. B.Z. also thanks Prof. Qingsong Tong at Fujian Normal University for valuable discussion.

References and Notes

(1) Hu, J.; Odom, T. W.; Lieber, C. M. *Acc. Chem. Res.* **1999**, *32*, 435.

(2) Xia, Y. N.; Yang, P. D.; Sun, Y. G.; Wu, Y. Y.; Mayer, B.; Gates, B.; Yin, Y. D.; Kim, F.; Yan, H. Q. *Adv. Mater.* **2003**, *15*, 353.

(3) Whitesides, G. M.; Grzybowski, B. *Science* **2002**, *295*, 2418.

(4) Iijima, S. *Nature (London)* **1991**, *354*, 56.

(5) Li, Y. D.; Li, X. L.; He, R. R.; Zhu, J.; Deng, Z. X. *J. Am. Chem. Soc.* **2002**, *124*, 1411.

(6) Suenaga, K.; Colliex, C.; Demoncy, N.; Loiseau, A.; Pascard, H.; Willaime, F. *Science* **1997**, *278*, 653.

(7) Huo, K. F.; Hu, Z.; Fu, J. J.; Xu, H.; Wang, X. Z.; Lu, Y. N. *J. Phys. Chem. B* **2003**, *107*, 11316.

(8) Hu, J. Q.; Bando, Y.; Zhan, J. H.; Liu, Z. W.; Golberg, D.; Ringer, S. P. *Adv. Mater.* **2005**, *17*, 975.

(9) Goldberger, J.; He, R.; Zhang, Y.; Lee, S.; Yan, H.; Choi, H. J.; Yang, P. *Nature (London)* **2003**, *422*, 599.

(10) Gates, B.; Mayers, B.; Cattle, B.; Xia, Y. N. *Adv. Funct. Mater.* **2002**, *12*, 219.

(11) Gates, B.; Yin, Y. D.; Xia, Y. N. *J. Am. Chem. Soc.* **2000**, *122*, 12582.

(12) Jiang, Z. Y.; Xie, Z. X.; Xie, S. Y.; Zhang, X. H.; Huang, R. B.; Zheng, L. S. *Chem. Phys. Lett.* **2003**, *368*, 425.

(13) Wang, X. J.; Zheng, X. W.; Lu, J.; Xie, Y. *Ultrason. Sonochem.* **2004**, *11*, 307.

(14) Mayers, B. T.; Liu, K.; Sunderland, D.; Xia, Y. N. *Chem. Mater.* **2003**, *15*, 3825.

(15) (a) Cheng, B.; Samulski, E. T. *Chem. Commun.* **2003**, 2024. (b) Tang, Z. Y.; Wang, Y.; Sun, K.; Kotov, N. A. *Adv. Mater.* **2005**, *17*, 358.

(16) Ren, L.; Zhang, H. Z.; Tan, P. G.; Chen, Y. F.; Zhang, Z. S.; Chang, Y. Q.; Xun, J.; Yang, F. H.; Yu, D. P. *J. Phys. Chem. B* **2004**, *108*, 4627.

(17) Xie, S. Y.; Wang, C. F.; Zhang, X. H.; Jiang, Z. Y.; Xie, Z. X.; Tian, Z. Q.; Huang, R. B.; Zheng, L. S. *J. Mater. Chem.* **2003**, *13*, 1447.

(18) (a) Cao, X. B.; Xie, Y.; Zhang, S. Y.; Li, F. Q. *Adv. Mater.* **2004**, *16*, 649. (b) Cao, X. B.; Xie, Y.; Li, L. Y. *Adv. Mater.* **2003**, *15*, 1914.

(19) Jiang, X. C.; Mayers, B.; Herricks, T.; Xia, Y. N. *Adv. Mater.* **2003**, *15*, 1740.

(20) Mayers, B.; Jiang, X. C.; Sunderland, D.; Cattle, B.; Xia, Y. N. *J. Am. Chem. Soc.* **2003**, *125*, 13364.

(21) Lu, J.; Xie, Y.; Xu, F.; Zhu, L. Y. *J. Mater. Chem.* **2002**, *12*, 2755.

(22) Ma, Y. R.; Qi, L. M.; Ma, J. M.; Cheng, H. M. *Adv. Mater.* **2004**, *16*, 1023.

(23) Chen, Y. T.; Sun, Q. Y.; Li, H. L. *Chem. Lett.* **2003**, *32*, 448.

(24) Zhang, H.; Yang, D. R.; Ji, Y. J.; Ma, X. Y.; Xu, J.; Que, D. L. *J. Phys. Chem. B* **2004**, *108*, 1179.

(25) Dai, G. P.; Liu, M.; Chen, D. M.; Hou, P. X.; Tong, Y.; Cheng, H. M. *Electrochem. Solid-State Lett.* **2002**, *5*, E13.

(26) Dai, G. P.; Liu, C.; Liu, M.; Wang, M. Z.; Cheng, H. M. *Nano. Lett.* **2002**, *2*, 503.

(27) Chen, J.; Kuriyama, N.; Yuan, H.; Takeshita, H. T.; Sakai, T. *J. Am. Chem. Soc.* **2001**, *123*, 11813.

(28) Chen, X.; Gao, X. P.; Zhang, H.; Zhou, Z.; Hu, W. K.; Pan, G. L.; Zhu, H. Y.; Yan, T. Y.; Song, D. Y. *J. Phys. Chem. B* **2005**, *109*, 11525.

(29) Tenne, R. *Angew. Chem., Int. Ed.* **2003**, *42*, 5124.

(30) Rajalakshmi, N.; Dhathathreyan, K. S.; Govindaraj, A.; Satishkumar, B. C. *Electrochim. Acta* **2000**, *45*, 4511.

(31) (a) Yannopoulos, S. N.; Andrikopoulos, K. S. *J. Chem. Phys.* **2004**, *121*, 4747. (b) Poborchii, V. V.; Kolobov, A. V.; Tanaka, K. *Appl. Phys. Lett.* **1999**, *74*, 215.

(32) Lee, S. M.; An, K. H.; Lee, Y. H.; Seifert, G.; Frauenheim, T. *J. Am. Chem. Soc.* **2001**, *123*, 5059.